Spins as Probes of Different Electronic States

DIETER SUTER, ROBERT KLIEBER

Universität Dortmund, Fachbereich Physik, 44221 Dortmund, Germany

ABSTRACT: Nuclear spins are efficient probes of electronic states. Because most NMR experiments are performed in thermal equilibrium, they probe the electronic ground state—the only state that is significantly populated under ambient conditions. Probing electronically excited states becomes possible, if magnetic resonance techniques are combined with optical (laser) excitation. Depending on the nature of the electronic state, drastic changes of the magnetic resonance parameters may be observed. We discuss the basic principles of this type of investigation. Depending on the lifetime of the electronically excited state, it is possible to measure separate spectra of ground and excited state if the lifetime is long on the NMR timescale, or an averaged spectrum if the lifetime is short. We present examples for both limiting cases using rare earth ions and semiconductor heterostructures. © 2007 Wiley Periodicals, Inc. Concepts Magn Reson Part A 30A: 116–126, 2007

KEY WORDS: nuclear spins; nuclear magnetic resonance; electronic state

INTRODUCTION

Since the first magnetic resonance experiments in condensed matter (*1–3*), research in magnetic resonance has grown to a large and diverse field, with applications ranging from science to medicine and engineering. Most of this research is driven by the possibility of using spins as probes of their environment, revealing details of structure (atomic, electronic, molecular) and dynamics. The relatively small energy scale of magnetic resonance implies that in most cases, the specific environment (e.g., strong magnetic field, radio-frequency irradiation) has only a small effect on the state of the material being investigated.

In this article, we discuss magnetic resonance (more specifically, nuclear magnetic resonance, NMR) investigations that probe the electronic state of some sample. The electronic state affects the NMR spectrum through different parameters, such as the chemical shift (*4*), the Knight shift (*5*), or the quadrupole interaction (*6*).

In most cases, the systems being investigated are in (or near) thermal equilibrium at temperatures of less than a few hunderd Kelvin. Accordingly, the electronic part of the system is then in its ground state and the NMR spectrum reflects the properties of the electronic ground state.

To probe a different electronic state, the system must be transferred into that state. This is possible by, for example, exciting an electronic transition with a laser field. Figure 1 shows an example: both spectra

Received 21 August 2006; revised 18 December 2006; accepted 8 January 2007

Correspondence to: Dieter Suter; E-mail: Dieter.Suter@Physik.Uni-dortmund.de

Concepts in Magnetic Resonance Part A, Vol. 30A(2) 116–126 (2007)

Published online in Wiley InterScience (www.interscience.wiley.com). DOI 10.1002/cmr.a.20076

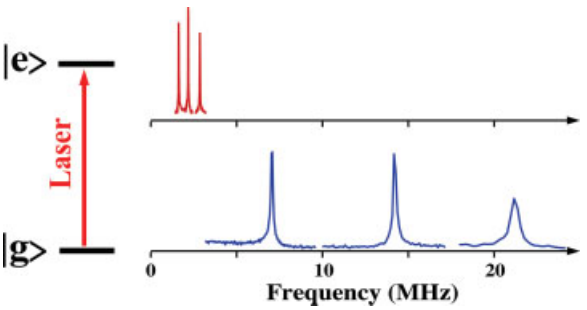

Figure 1 Evidence for the drastic changes that can occur in an NMR spectrum when the electronic state changes. Both spectra are from the same nuclear spin, in the same sample, at the same lattice site. The only difference is the electronic state. [Color figure can be viewed in the online issue, which is available at www.interscience.wiley.com.]

were taken from the nuclear spin transitions of ^{141}Pr, which was included as a dopant in the host material $YALO_3$. Resonant absorption of light from a laser beam caused these ions to change the electronic state between the ground state and an electronically excited state. The lower spectrum (blue in the online version) originates from those ions that are in the electronic ground state, whereas the upper (red) spectrum is from the electronically excited ions. The position of the resonance lines is determined by the nuclear quadrupole interaction, which changes by almost an order of magnitude when the electronic state changes.

Though it is in principle possible to change the electronic state by optical irradiation and use conventional NMR for observing the changes, it is in most cases advantageous to use the same laser that drives the electronic state change also for excitation and detection of the magnetic resonance spectra. This approach may be necessary if the population of the excited state is too small to yield a detectable signal in conventional NMR.

A number of different experimental procedures have been demonstrated that use optical radiation for excitation or detection of magnetic resonance. Many review articles are available that cover these techniques (see, e.g., *7*, *8*)

RAMAN-HETERODYNE DETECTION OF NMR

One of the experimental approaches that use lasers for the detection of magnetic resonance is the Raman heterodyne experiment (*9*, *10*). Figure 2 illustrates the relevant processes. The upper part shows the radio-frequency photon emitted by the NMR transition. In conventional NMR, we detect this photon by using a tuned radio-frequency (RF) circuit as an antenna. In Raman heterodyne detection, we add it to an optical photon (energy $\hbar\omega_{Las}$) to generate a frequency-shifted optical photon whose energy is the sum or the difference of the energy of the incident optical photon and the RF photon ($\hbar\omega_{RF}$). Such optical photons can be detected with high efficiency and sensitivity. It is an optical analog of the mixing process that is used in every NMR (and ESR) spectrometer.

The lower part of Fig. 2 shows the associated experimental setup: an RF field excites transverse magnetization (= coherence) in an NMR transition. Simultaneously, a laser couples to an optical transition that shares a state with the NMR transition to be detected. The combined effect of these two electromagnetic fields is that coherence is excited in all three transitions of the three level system. This includes the two transitions to which the RF and optical fields couple, but also the third transition, which did not interact with any field. If this third transition is associated with an electric dipole transition, this coherence corresponds to an oscillating electric dipole.

Such an optical polarization is the source of an optical field. Because its frequency is shifted from the frequency of the incident laser field, it is termed a Raman field. Whereas the conventional Raman effect generates spontaneously emitted photons, the process described here creates a Raman field whose phase $\phi_R = \phi_L \pm \phi_{RF}$ is given by the sum of the phases of the two driving fields. This well-defined phase

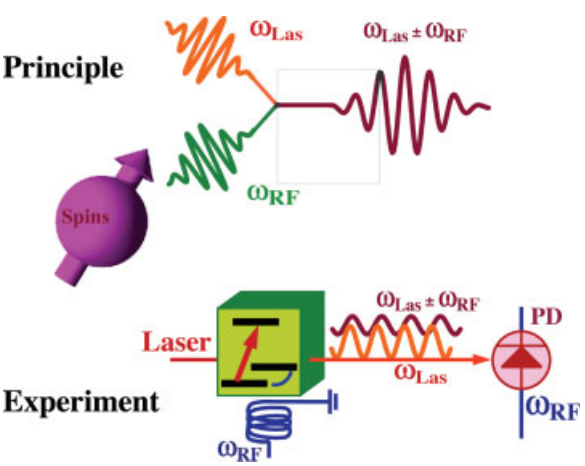

Figure 2 Coherent Raman scattering for the detection of magnetic resonance. [Color figure can be viewed in the online issue, which is available at www.interscience.wiley.com.]

relation makes detection significantly easier. To emphasize this distinction, this process is often termed a "coherent Raman process."

The emitted Raman field propagates in the same spatial direction as the incident laser field. This permits a relatively straightforward detection scheme: The two optical fields are focused on a photodiode. Like most optical detectors, photodiodes produce an electrical signal that is proportional to the optical power incident on the photodiode. The signal can thus be written

$$s \propto |E|^2 = |E_L + E_R|^2 = |E_L|^2 + |E_R|^2 + 2|E_L E_R|,$$

where E_L is the laser and E_R the Raman field. The first two terms, which represent the intensity of the laser and Raman fields, do not depend on time. The third term, which represents an interference term between the two fields (remember that they have a well-defined phase relation) oscillates at the difference frequency of the two fields,

$$|\omega_R - \omega_L| = \omega_{RF},$$

(i.e., at the radio frequency corresponding to the NMR transition). This signal can thus be treated like a conventional NMR signal, feeding it to a phase-sensitive detector. The experiment can be performed in the frequency domain, measuring the signal as a function of a slowly varying rf frequency or in the time domain, Fourier transforming the free induction decay to obtain an NMR spectrum.

LONG-LIVED ELECTRONIC STATES

We now compare Raman heterodyne spectra of distinct electronic states in the limit of long lifetimes. This corresponds to the slow-exchange limit, where each site yields a separate spectrum. For each subspectrum, the signal strength depends on the population of the corresponding electronic state as well as the relevant transition matrix elements, which may also be specific for the states.

System and Hamiltonian

For the specific examples, we chose the rare earth ion $^{141}Pr^{3+}$, whose electronic states have lifetimes of >100 μs. All the relevant optical transitions in this system are "forbidden" transitions (i.e., they occur between different spin states) between states of equal parity and/or they change the angular momentum by more than one unit. However, the number of electronic states is large, and the couplings between them are strong enough to significantly mix these states. As a result, optical transitions can be excited between all states. The optical transitions are relatively narrow, with an inhomogeneous broadening of about 5 GHz and homogeneous optical linewidths of less than 100 kHz. Optical excitation is achieved with a tunable dye laser.

^{141}Pr has a nuclear spin of $I = 5/2$ and is doped into a lattice of $YAlO_3$, where it replaces some of the yttrium ions. Because these two ions have the same charge and similar size, the lattice distortion caused by this random doping mechanism is small.

The site of the ion has a low symmetry (C_{1h}) (*11–13*) with a significant electric field gradient. As a result, the nuclear spin states split into three doubly degenerate pairs of states. Each pair consists of two states with opposite m_z values (i.e., $m_z = \pm\frac{1}{2}, \pm\frac{3}{2}, \pm\frac{5}{2}$).

The electronic states that we compare here are the electronic ground state, which has the term symbol $^3H_4$, and an electronically excited state with the term symbol $^1D_2$. In both states, 54 electrons occupy the states of the rare gas Xe, and two additional electrons occupy 4*f* levels. The only difference between these two states is that in the ground state, the two f electrons obey Hund's rule (i.e., they have parallel spins and maximal orbital angular momentum ($L = 5$), whereas in the excited state their spins are paired and the orbital angular momentum is reduced to $L = 2$ (*13*). The two states are separated by an energy of 2.03 eV; the transition can therefore be excited by a laser with a wavelength of 611 nm.

The nuclear quadrupole coupling lifts the degeneracy of the nuclear spin states. The splittings, which are determined by the quadrupole coupling constant, vary with the electronic state. Figure 3 shows the relevant part of the energy-level scheme of the $^3H_4$ and $^1D_2$ states. As shown in the figure, the nuclear quadrupole coupling differs for the two states by almost an order of magnitude. For the electronic ground state, the splittings are 7.1, 14.1, and 21.2 MHz. For the electronically excited state, the corresponding values are 0.85, 1.55, and 2.4 MHz (*14*). The corresponding coupling constants are listed in Table 1, together with the principal components of the gyromagnetic tensors for the states (*12*, *15*).

Pure Quadrupole Spectra

The righthand side of Fig. 3 shows the optically detected pure NQR (i.e., $B = 0$) spectra for the two electronic states. All experiments discussed here are performed at liquid helium temperatures. Depending

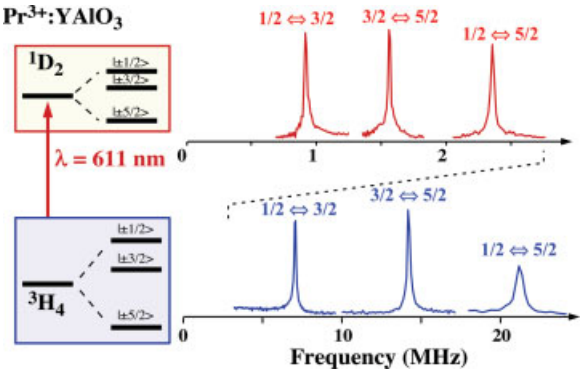

Figure 3 Energy level scheme of the nuclear spin states in the two different electronic states being discussed. The upper trace shows the (optically detected) NQR spectrum of the electronically excited state, the lower part that of the electronic ground state. Note the different scale of the two spectra and the two energy level schemes. [Color figure can be viewed in the online issue, which is available at www.interscience.wiley.com.]

on the details of the experiment, optimal temperatures range from 3 to 12 K. In both spectra, the three resonance lines that can be observed correspond to the three nondegenerate transitions within the nuclear spin levels and are labeled with the m_z values of the states. Due to limitations in the spectral range, the three transitions had to be measured in separate experiments (*16*). Though the $\pm 1/2 \leftrightarrow \pm 5/2$ transition is not normally observed in directly detected NMR (two-quantum transition), the optical excitation and detection procedure used in this case also excites this transition (*16*).

NMR Spectrum

When a magnetic field is applied to the system, it lifts the remaining twofold degeneracy of the nuclear spin states, and the nuclear spin transitions split into four. Figure 4 shows how the nuclear spin states split in a magnetic field of some 10 mT. On the righthand side, the corresponding NMR spectrum is shown, consisting of eight resonance lines. Apart from the dipole-allowed transitions $-1/2 \leftrightarrow -3/2$ and $+1/2 \leftrightarrow +3/2$, we also observe the $-1/2 \leftrightarrow +3/2$ and $+1/2 \leftrightarrow -3/2$ transitions. The apparent breaking of the magnetic dipole selection rules is an indication that the nominal $\pm 1/2$ and $\pm 3/2$ states are mixed with each other as well as with the $\pm 5/2$ states. This is a consequence of the asymmetric terms of the quadrupole coupling Hamiltonian as well as of the static magnetic field, which has, at this orientation, off-digaonal elements with respect to the principal axis system of the electric field gradient tensor.

Each nuclear spin therefore contributes four resonance lines to the spectrum. The total of eight lines visible in the spectrum of Fig. 4 arises from two nonequivalent sites. Of the four possible sites in the unit cell of $YAlO_3$, two are nonequivalent if the magnetic field is in a general orientation. They therefore show different splittings, leading to a total of eight resonance frequencies (*12*, *17*, *18*). The numbers in the energy level diagram and near the resonance lines identify the different transitions for both sites.

An interesting feature of this Raman heterodyne spectrum is that four of the resonance lines have positive amplitude, whereas the remaining four lines have negative amplitude. This is not an effect of negative spin temperature, but can be traced to the dependence of the Raman heterodyne signal on the transition matrix elements. In a conventional NMR experiment, the amplitude of a resonance line is proportional to

$$s_{NMR} \propto |I_x^{rs}|^2,$$

where I_x is the transverse spin operator and the index^{rs} refers to the matrix element of the transition being observed. In a Raman heterodyne experiment, however, three transitions are involved: the nuclear spin transition, the transition to which the laser couples, and the Raman transition where the frequency-shifted field is emitted. The resulting signal amplitude is proportional to the product of the transition matrix elements in all three transition,

$$s_{RHS} \propto I_x^{rs} \mu^{st} \mu^{tr},$$

where μ is the electric dipole operator for the two optical transitions.

Though it is possible to choose the phase of each state such that individual transition matrix elements become real and positive, the triple product is invariant under such transformations. For the specific case of Pr:$YAlO_3$, it has been shown that the triple prod-

Table 1 Quadrupole Couplings Constants D(= ω_q) and E(= $\eta\omega_q/3$), and Gyromagnetic Ratios of the Pr^{3+}:YA1O_3 Hamiltonian of the Pr^{3+} $^3H_4$ Ground State at 3 K and $^1D_2$ Excited State at 12 K

State	D [MHz]	E [MHz]	$\gamma_x/2\pi$ [kHz/G]	$\gamma_y/2\pi$ [kHz/G]	$\gamma_z/2\pi$ [kHz/G]
$^3H_4$	−3.5289	−0.0118	3.5	2.43	11.05
$^1D_2$	−0.4024	−0.0512	1.48	1.57	1.57

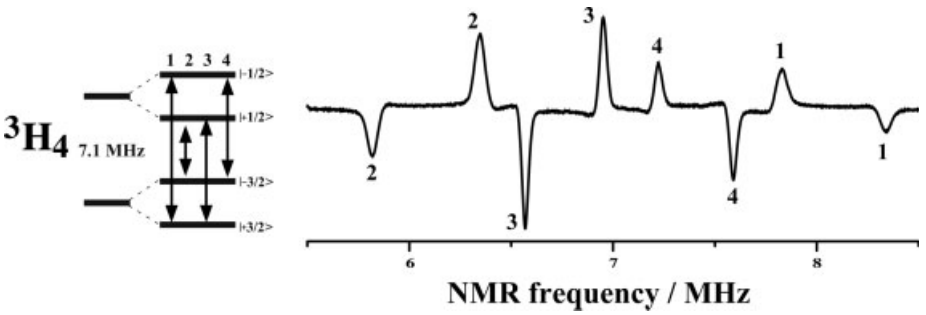

Figure 4 Splitting of the $\pm\frac{1}{2}$ and $\pm\frac{3}{2}$ nuclear spin states in a magnetic field and the corresponding Raman heterodyne-detected NMR spectrum.

uct has opposite sign for the two crystallographically nonequivalent sites. The positive lines therefore are associated with one site (we will refer to it from now on as site 1), and the negative lines are associated with the other site (site 2) (*12*, *19*).

CORRELATION SPECTROSCOPY

The Problem

According to the argument given above, an ion contributes to the NMR subspectrum with the positive or with the negative lines, depending on which crystallographic site it is located. When the ion is in the excited state, its NMR spectrum changes, and all eight line positions switch to a frequency range around 1 MHz.

Figure 5 shows a part (around 7.1 MHz) of the NMR spectrum of the electronic ground state along the horizontal axis and a part (around 0.9 MHz) of the excited-state spectrum along the vertical axis. Within each spectrum, the resonance lines with the same sign arise from the same nuclear spins. At this stage, however, we do not know which of the two excited-state subspectra can be attributed to which ground-state subspectrum. If we refer to the ground-state subspectra as 1g and 2g and to the excited-state subspectra as 1e and 2e, we are left with two possibilities: (a) one nuclear site yields the spectra 1g and 1e, the other site 2g and 2e or (b) one nuclear site yields the spectra 1g and 2e, the other site 2g and 1e.

The Correlation Experiment

To decide between these two possibilities, we perform a 2D correlation experiment. Figure 6 shows the pulse sequence that correlates the NMR spectra of two different electronic states (*20*). We discuss the principle with the help of the simplified energy level scheme shown in the lefthand part of Fig. 6.

The experiment starts in thermal equilibrium, where only the electronic ground state is populated. A laser π pulse then transfers population from the electronic ground state to the electronically excited state. Ideally, this laser pulse populates only one of the nuclear spin states of the excited state, yielding a highly (i.e., almost 100%) polarized nuclear spin system.

A resonant RF pulse converts the population difference between the two nuclear spin states of the electronically excited state into transverse magnetization that is allowed to precess freely under the internal Hamiltonian of the system. After the evolution time t_1, a second RF pulse converts the transverse magnetization back into population difference within the electronically excited state. This population dif-

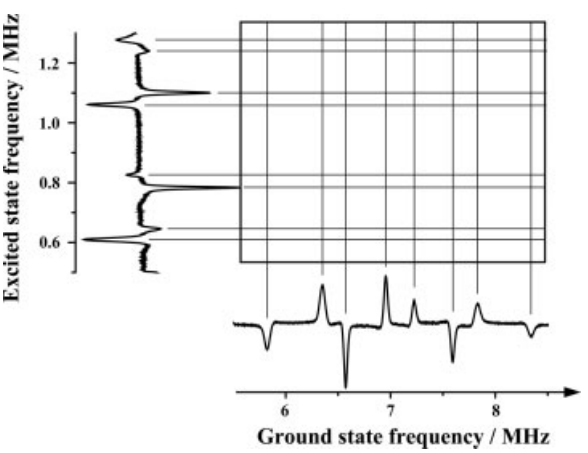

Figure 5 Raman heterodyne-detected NMR spectrum of the electronically excited state (left) and of the electronic ground state (bottom). The rectangle indicates the possible positions of resonance lines in a 2D correlation spectrum. Each of the two sites contributes to 16 resonance lines in the 2D spectrum. For the two sites, we therefore expect 32 resonance lines, half of the 64 possible positions.

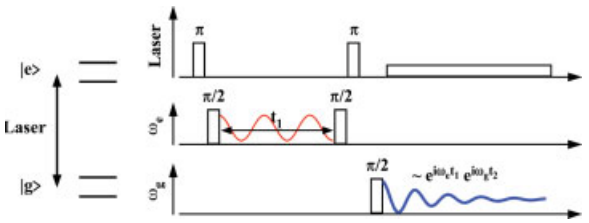

Figure 6 Simplified energy level system for the correlation experiment and pulse sequence used to correlate the subspectra of the electronic ground state with those of the excited state. The upper trace shows the laser pulses, the middle and lower trace the radio-frequency pulses applied to the excited and ground state. [Color figure can be viewed in the online issue, which is available at www.interscience.wiley.com.]

ference is therefore modulated by $e^{i\omega_e t_1}$, where $\hbar\omega_e$ is the splitting between the two nuclear spin states.

A second laser pulse that exchanges the populations of the ground and excited state brings this population difference into the ground state. A final RF pulse, this time resonant with the ground-state NMR transition, turns the population into precessing magnetization, which then is read out by a Raman heterodyne process stimulated by the weak laser field shown in the uppermost trace of Fig. 6.

The resulting signal is thus proportional to

$$s_1(t_1, t_2) = \cos(\omega_e t_1) e^{-i\omega_g t_2}. \qquad [1]$$

Fourier transformation of this signal yields a resonance line in the 2D spectrum at position $(\omega_1, \omega_2) = (\omega_e, \omega_g)$.

Experimental Example

For a specific example, we consider the $Pr{:}YAlO_3$ system discussed above, taking the $\pm\frac{1}{2}$ and $\pm\frac{3}{2}$ nuclear spin states into account in both electronic states. The individual NMR spectra (in nonzero magnetic field) thus consist of four transitions in the electronic ground state and four transitions in the electronically excited state. The experiment correlates each of these ground-state transitions with the excited-state transitions of the same spin. For each spin species, we thus expect 16 lines in the 2D spectrum. For the two sites, a total of 32 2D resonances are expected at the 64 possible positions.

Experimentally, the two RF pulses cannot excite the full frequency range. We therefore have to select a section of the 2D spectrum.

Figure 7 shows an example of such a 2D correlation spectrum. The left-hand part indicates the section of the full 2D spectrum that is represented in the right-hand part of the figure. The part of the 2D spectrum shown here covers 8 of the 64 frequency positions. The experimental spectrum in the right-hand part indicates signals at four of these positions. The relatively large differences between the amplitudes is mostly due to off-resonance effects, which result for example, in the low excitation efficiency of the line at $\omega_2 = 8.2$ MHz.

Using different frequencies for the RF pulses, different parts of the full 2D spectrum could be covered. Figure 8 shows the summary of four such spectra. The full circles indicate the observed resonance lines. They are consistent with one of the two possible assignments: Subspectrum 1g corresponds to 1e and

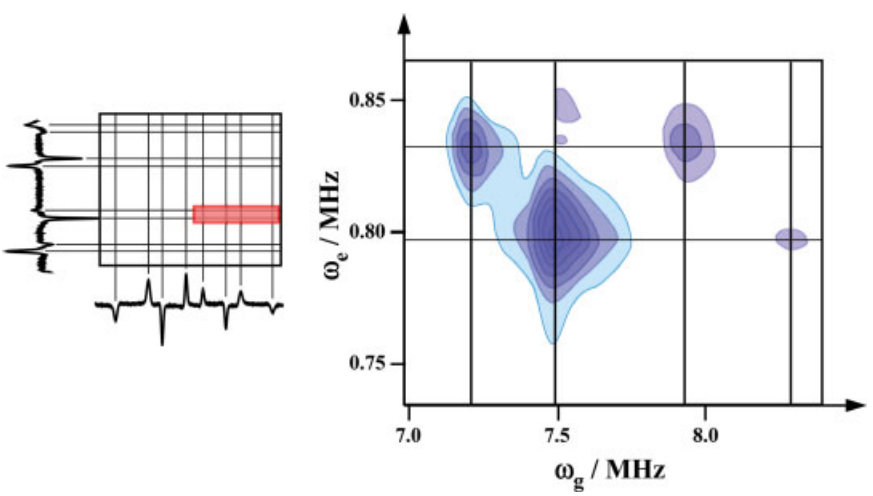

Figure 7 Experimental correlation spectrum using rf frequencies 0.85 and 7.50 MHz for the excited and ground state, respectively. [Color figure can be viewed in the online issue, which is available at www.interscience.wiley.com.]

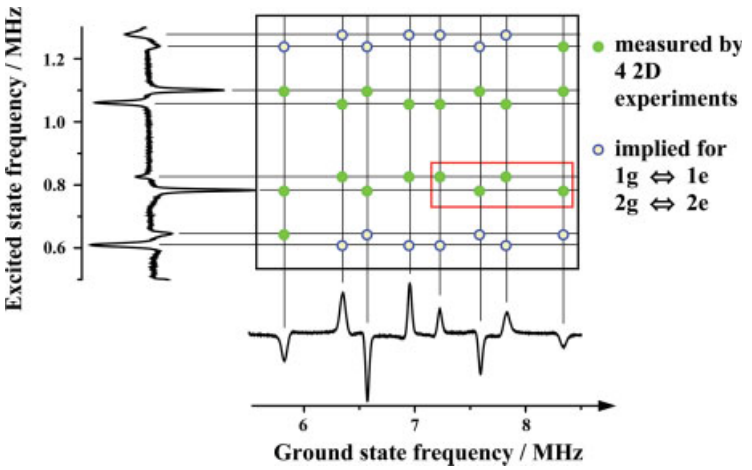

Figure 8 Complete 2D correlation spectrum. The rectangle indicates the position of the spectrum of Fig. 7. The full circles indicate the positions of the resonances found in a total of four 2D correlation experiments. The empty circles indicate additional positions in ranges not covered by the experiments. The full and empty circles together are the positions expected if the 1g subspectrum originates from the same spins as the 1e subspectrum and the 2g corresponds to the 2e subspectrum. [Color figure can be viewed in the online issue, which is available at www.interscience.wiley.com.]

subspectrum 2g to 2e. If we accept this assignment, then we expect additional resonance lines in the region not covered by the experiments. These implied peaks are shown by empty circles. The full and empty circles together cover half of the possible peak positions in the full 2D correlation spectrum.

FAST EXCHANGE LIMIT: GaAs

We now consider the opposite limit where the lifetime of the electronic states is short on the NMR time scale. The system thus switches between the two states (usually spending more time in the ground state than in the excited state), and the NMR spectrum that we observe is an averaged spectrum rather than two distinct spectra. The system that we discuss here is a semiconductor, specifically GaAs quantum films. For this system, the lifetime of the electronically excited state is <1 *ns* (i.e., much shorter than any relevant NMR timescale).

In this system, three different nuclear spin species can be used to probe the electronic state: ^{69}Ga, ^{71}Ga, and ^{75}As. Each of these has a spin $I = \frac{3}{2}$ and can thus probe the environment through the Zeeman as well as the quadrupole interaction.

The two interactions can probe different properties of their environment: The quadrupole coupling is proportional to the electric field gradient (i.e., to the asymmetry of the charge distribution in the vicinity of the nucleus). In the case of GaAs, the structure has cubic symmetry and therefore a vanishing electric field gradient.

In a real structure—in particular in quantum films—where the symmetry is lower than in an ideal bulk crystal, the NMR spectra show nonvanishing quadrupole splittings, indicating that the electric field gradient is nonzero. This finding can be tracked to two related causes of geometrical (lattice) distortion and to electronic effects. A distortion of the nuclear lattice, either due to macroscopic or microscopic effects, has been studied in different systems (*21–24*). Here, we concentrate instead on electronic effects. As the site symmetry of the nuclei does not include an inversion center, an electric field can induce an electric field gradient that causes a quadrupole splitting.

Such electric fields can be applied externally, or they can arise within the material. An example is the Schottky effect: If a layer of metallic material is in contact with a semiconductor, a transfer of electrons occurs between the two materials that creates an electric field. The electric field vanishes as a result of local charge depletion over a depth of the order of 1 μm.

Figure 9 shows an example. A layer of transparent electrode material InSnO was deposited on top of a semiconductor sample containing several GaAs quantum wells. The Schottky barrier created by this arrangement is an electric field that varies over a distance of approximately 1 μm. To probe the variation of this electric field, spectra of Ga and As were measured. To obtain the necessary depth resolution, a

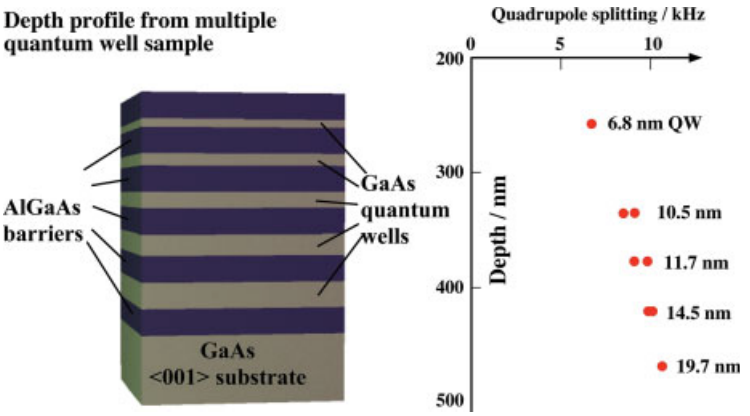

Figure 9 Multiple quantum well sample. Optically detected NMR spectra were taken of the different GaAs quantum wells. The measured quadrupole splitting varies with the distance of the quantum well from the top of the sample. [Color figure can be viewed in the online issue, which is available at www.interscience.wiley.com.]

sample with different quantum wells was used. By adjusting the laser frequency to the resonance of each quantum well, it is possible to choose which specific quantum well is excited. Only the nuclear spins within this thin film (layer thickness 5–20 nm) are excited and contribute to the signal. The observed change of the quadrupole splittings is compatible with an internal electric field that changes with depth z as

$$E^s(z) = 2\Phi_0 \frac{d-z}{d^2},$$

where d is the depth of the Schottky layer and the expression holds for $z < d$.

KNIGHT SHIFT

Knight Shift and Electronic States

The relevant optical transition of GaAs couples the electronic ground state (= valence band) with the first excited state (= conduction band).

The main difference between the ground and excited state is the character of the orbitals, as shown in Fig. 10. Whereas the valence band consists of p-type orbitals, the conduction band is built of s-orbitals. This means that-the electron density at the position of the nuclei is qualitatively different. The hyperfine interaction between the electronic and nuclear spin is directly proportional to the electron density, $A \propto n(\vec{r_n})$, where n is the electron density and $\vec{r_n}$ the position of the nucleus.

In a static picture, we would expect that the hyperfine interaction causes a splitting in the NMR spectrum, with the separation between the two subspectra given by the hyperfine coupling constant A. However, since the lifetime of the electronically excited state is less than 1 *ns*, the system is in the fast exchange limit where the two subspectra collapse into one, which is located at the average position of the two. At higher temperatures and different excitation conditions, the photogenerated carriers also become mobile, thus providing an even faster averaging mechanism. If the population of the two electron spin states is equal, the average spectrum is not distinguishable from a spectrum of a system with vanishing hyperfine interaction.

If, however, the population of the two electron spin states is not the same (i.e., if the conduction band electrons are spin polarized), the two subspectra have different amplitudes and the average is shifted toward the more populated state.

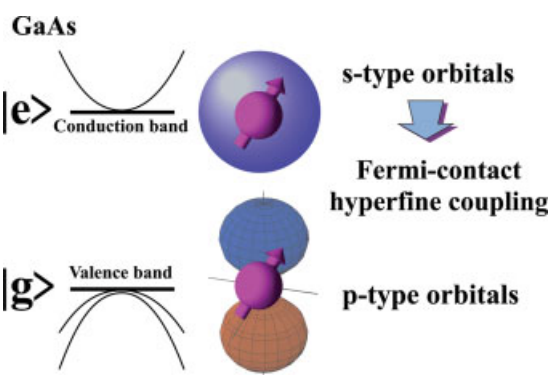

Figure 10 Comparison of the orbital structure of the conduction band and valence band of GaAs. [Color figure can be viewed in the online issue, which is available at www.interscience.wiley.com.]

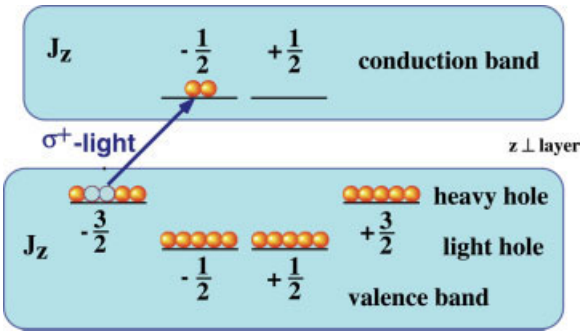

Figure 11 Selection rules and generation of spin-polarized conduction band electrons by absorption of circularly polarized (σ_+) light. In the ground state, the degeneracy of the (electronic) angular momentum states is lifted in the quantum well. [Color figure can be viewed in the online issue, which is available at www.interscience.wiley.com.]

Such an effect can be observed in metals, where the NMR frequency shifts as a function of the spin polarization of the conduction electrons. This effect was first described by Knight (*5*) and is called the Knight shift. The Knight shift is proportional to the hyperfine coupling constant (and thus to the electron density) and to the spin-polarization $\langle S_z \rangle$, $\delta_K \propto n\langle S_z \rangle$. Because the density of conduction electrons is small in semiconductors, the Knight shift is usually not observable.

Optically Generated Electron Spin Density

In our system, the conduction band electrons are created by absorption of light from a resonant laser beam. As shown in Fig. 11, it is possible to generate fully spin-polarized electrons by tuning the laser wavelength to the transition between the $m_J = \frac{3}{2}$ states (= "heavy hole") and the conduction band orbitals and using circularly polarized light. For this choice of optical radiation, only the transition from the $m_J = -\frac{3}{2}$ ground state to the $m_J = \frac{1}{2}$ excited state is allowed, and the newly created conduction electrons are all in the $m_J = -\frac{1}{2}$ state. By adjusting the polarization of the photons, the electron spin polarization can be varied. The electron density is determined by the intensity of the light. Controlling these two parameters, it is therefore possible to optically create a Knight shift between a minimal and a maximal value determined by the laser intensity.

Experimental Example

Figure 12 shows an example: The nuclear spins of a GaAs quantum well were first polarized by optical pumping (*25*). A $\frac{\pi}{2}$ RF pulse then converted the polarization of the ^{75}As nuclear spins into transverse magnetization, which was allowed to precess in an external magnetic field. The precession was monitored through its effect on the polarization of the photoluminescence, which yields a signal that is equivalent to an FID (*25*). This signal was then Fourier transformed to yield the spectra shown in Fig. 12.

All three spectra show a splitting due to quadrupole coupling (resulting from strain), which does not change under the effect of the optical irradiation. The light does, however, cause a shift of all three lines by an amount that is proportional to the intensity of the optical irradiation and thus of the excited state population and electron spin density (*26*). Inverting the polarization of the light from right to left circular polarization inverted the sign of the Knight shift.

One difficulty with this measurement is that the optical radiation is used for two purposes—to generate the electron spin density and thus the Knight shift, but also to induce the photoluminescence that provides the detection signal. Changing the intensity or polarization of the light therefore affects the precession frequency as well as the detection efficiency.

One way to avoid this problem is to separate the two processes in the form of a 2D experiment. For this purpose, the Knight shift is generated by optical irradiation during the evolution period of the 2D experiment, while the spins are allowed to precess, as shown in the upper part of Fig. 13. For the detection period, the optical radiation is switched to a standard setting.

In the resulting 2D spectrum, shown in the lower part of Fig. 13, the Knight shift can be measured as

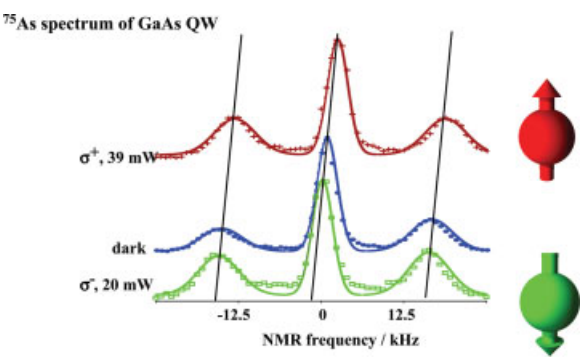

Figure 12 NMR spectrum of ^{75}As nuclear spins in a quantum well in the presence of positive (upper trace), negative (lower trace), and vanishing electron spin polarization showing the optically induced Knight shift. The red and green spectra are offset vertically from the blue (dark) spectrum by an amount proportional to the laser intensity. [Color figure can be viewed in the online issue, which is available at www.interscience.wiley.com.]

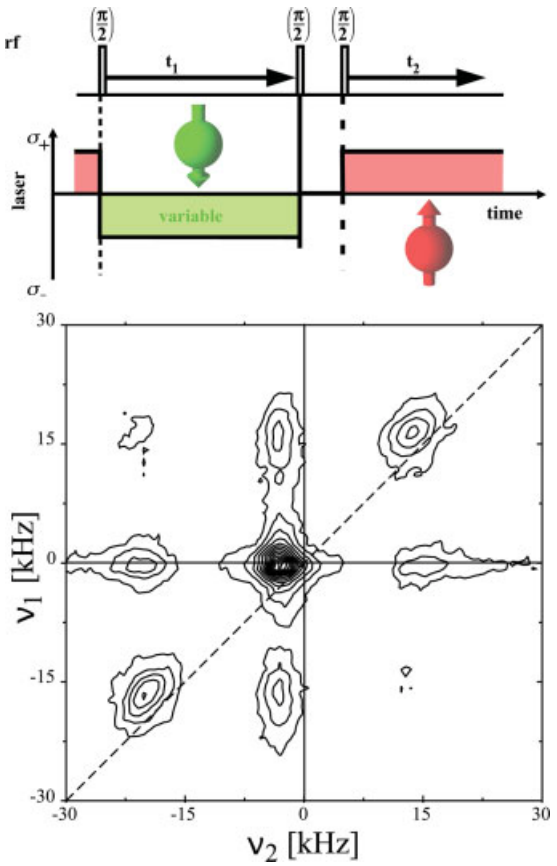

Figure 13 Two-dimensional experiment for the measurement of the optically induced Knight shift. The upper part shows the pulse sequence, where the optical irradiation during evolution and detection may have different values. The lower part shows an example of a resulting spectrum. [Color figure can be viewed in the online issue, which is available at www.interscience.wiley.com.]

the difference in the frequency during the evolution and detection period, which correspond to the vertical and horizontal axis. In the example shown in Fig. 13, the optical polarization was switched from σ_- during the evolution period to σ_+ during the detection period. As a result, the Knight shift-changed sign and the lines in the 2D spectrum are shifted away from the diagonal, where they would appear if the frequencies were constant. The distance of the resonance lines from the diagonal (dashed line) measures the change in the Knight shift.

CONCLUSION

Many different applications of NMR have been developed to probe the properties of electronic states in different systems. In most cases, the system is in the electronic ground state. Here, we have shown that NMR can also be used to probe properties of electronically excited states. In the context of this conceptual overview, we have concentrated on two different systems that represent two extreme examples: in the case of rare earth ions, the long excited state lifetimes allow one to observe the NMR spectra of different states independently. The observed splittings and transition strengths can be used to extract detailed information about the electronically excited state: the quadrupole coupling constant as well as the enhanced gyromagnetic ratio are determined by the electronic state (*27*). The nominal state is mixed with a number of different states, and the electronic angular momentum is quenched by the crystal field.

In the case of GaAs, the short lifetime implies that all NMR measurements observe only the time average of the two relevant electronic states. Variation of the optical power (and therefore the relative occupation numbers of the two states) allows one, to some degree, to extract the individual parameters. In particular, the observed Knight shift is a direct measure of the electronic spin polarization, the lifetime of the electron spin, and the electronic excitation (*26*).

ACKNOWLEDGMENTS

Many people have contributed to the work discussed here. Among the most important contributors were Jürgen Mlynek, Tilo Blasberg, Rudolf Neuhaus, Greg Flinn, and Marcus Eickhoff. The work was supported by the DFG through various grants.

REFERENCES

1. Bloch F. 1946. Nuclear induction. Phys Rev 70:460.
2. Purcell EM, Torrey HC, Pound RV. 1946. Resonance absorption by nuclear magnetic moments in a solid. Phys Rev 69:37.
3. Zavoisky E. 1945. Spin-magnetic resonance in paramagnetics. J Phys 9:245.
4. van Beek JD, Beaulieu L, Schfer H, Demura M, Asakura T, Meier BH. 2000. Solid-state NMR determination of the secondary structure of Samia cynthia ricini silk. Nature 405:1077.
5. Knight WD. 1949. Nuclear magnetic resonance shift in metals. Phys Rev 76:1259.
6. Klieber R, Michalowski A, Neuhaus R, Suter D. 2003. Nuclear quadrupole resonance of an electronically excited state from high-resolution hole-burning spectroscopy. Phys Rev B-67:184103.
7. Suter D, Mlynek J. 1991. Laser excitation and detection of magnetic resonance. Adv Magn Opt Reson 16: 1–83.

8. Suter D. 1996. Optically enhanced magnetic resonance. In: Grant DM, Harris RK, editors. Encyclopedia of NMR. Conchester: Wiley. p 337.
9. Garmire E, Pandarese F, Townes CH. 1963. Coherently driven molecular vibrations and light modulation. Phys Rev Lett 11:160.
10. Giordmaine JA, Kaiser W. 1966. Light scattering by coherently driven lattice vibrations. Phys Rev 2:676.
11. Diehl R, Brandt G. 1975. Crystal structure refinement of $YA1O_3$, a promising laser material. Mater Res Bull 10:85.
12. Mitsunaga M, Kintzer ES, Brewer RG. 1985. Raman heterodyne interference: observations and analytic theory. Phys Rev B 31:6947.
13. Erickson LE. 1979. Hyperfine interaction in the lowest levels of the $^3H_4$ and $^1D_2$ states of trivalent praseodymium in yttrium aluminum perovskite (YA1O3). Phys Rev B 19:4412.
14. Erickson LE. 1977. Optical measurement of the hyperfine splitting of the $^1D_2$ metastable state of Pr^{3+} in LaF_3 by enhanced and saturated absorption spectroscopy. Phys Rev B 16:4731.
15. Blasberg T, Suter D. 1995. Determination of oscillator strengths in Pr^{3+}:$YA1O_3$ by Raman heterodyne and hole burning spectroscopy. J Lumin 65:199.
16. Blasberg T, Suter D. 1994. Determination of oscillator strengths in Pr^{3+} $YA1O_3$ by Raman heterodyne and hole burning spectroscopy. Optics Commun 109:133.
17. Erickson LE. 1990. Optical pumping effects on Raman-heterodyne-detected multipulse rf nuclear-spin-echo decay. Phys Rev B 42:3789.
18. Mitsunaga M, Kintzer ES, Brewer RG. 1984. Raman heterodyne interference of inequivalent nuclear sites. Phys Rev Lett 52:1484.
19. Kintzer ES, Mitsunaga M, Brewer RG. 1985. Raman heterodyne intereference: symmetry analysis. Phys Rev B 31:6958.
20. Klieber R, Suter D. 2005. Correlating NQR transitions of ground and excited electronical states. Phys Rev B 71:224418.
21. Flinn GP, Harley RT, Snelling MJ, Tropper AC, Kerr TM. 1990. Optically detected nuclear magnetic resonance in semiconductor quantum wells. J Luminesc 45:218.
22. Carlos WE, Bishop SC, Treacy DJ. 1991. Nuclear-magnetic-resonance studies of strain in isovalently doped GaAs. Phys Rev B 43:12512.
23. Guerrier DJ, Harley RT. 1997. Calibration of strain vs nuclear quadrupole splitting in III–V quantum wells. Appl Phys Lett 70:1739.
24. Eickhoff M, Lenzmann B, Suter D, Hayes SE, Wieck AD. 2003. Mapping of strain and electric fields in GaAs/AlGaAs quantum-well samples by laser-assisted NMR. Phys Rev B 67:085308.
25. Eickhoff M, Suter D. 2004. Pulsed optically detected NMR of single GaAs/AlGaAs quantum wells. J Magn Reson 166:69.
26. Eickhoff M, Fustmann S, Suter D. 2005. Light-induced Knight shifts in GaAs/AlGaAs quantum wells. Phys Rev B 71:195332.
27. Bleaney B. 1973. Enhanced nuclear magnetism. Physica 69:317.

BIOGRAPHIES

Dieter Suter studied chemistry at ETH Zürich and did his PhD work with Richard Ernst in solid-state NMR. He did postdoctoral research with Alex Pines (UC Berkeley) and then moved to the physics department of ETH, where he worked in quantum optics with Jürgen Mlynek. In 1995, he became professor of condensed matter physics at the University of Dortmund. His current research interests include magnetic resonance and optical spectroscopy of hard and soft matter.

Robert Klieber studied physics at the University of Dortmund, Germany, and received his PhD (2005) in Dortmund in the group of Prof. Dieter Suter. The focus of his PhD thesis was mainly the development of optical NMR detection techniques. He is currently working within the technology and development group for CMOS technology at the Fraunhofer Institute of Microelectronic Circuits and Systems in Duisburg, Germany.